

# DEVELOPMENT AND SIMULATION OF NONLINEAR AEROELASTIC ANALYSIS SYSTEM FOR ADVANCED TRANSONIC AIRCRAFTS

I. Lee<sup>1</sup>, J.-Y. Kim<sup>2</sup>, K.-S. Kim<sup>2</sup>

Dept. of Aerospace Engineering, Korea Advanced Institute of Science and Technology  
335 Gwahangno, Yuseong-gu, Daejeon 305-701  
Republic of Korea

## OVERVIEW

The aeroelastic analysis system has been developed using the coupled techniques of computational fluid dynamics (CFD) and computational structural dynamics (CSD) in the present study. The analysis system is applied to the several aircraft models with structural and aerodynamic nonlinearities. The restoring force vector is considered in the equation of motion to perform the aeroelastic analysis with concentrated structural nonlinearity such as freeplay. The effects of control surface freeplay on the aeroelastic characteristics are investigated. For the aircraft model with high-aspect-ratio wing, the aeroelastic analysis is performed using the structural analysis based on large deflection beam theory. On the other hand, the transonic small disturbance (TSD) code is used for the nonlinear aerodynamic analysis in the transonic region. The nonlinear aeroelastic analysis using the TSD theory is performed for the full aircraft model including the body, main wings, horizontal tails, vertical fin, launchers and several control surfaces.

## 1. INTRODUCTION

The aircrafts always have aeroelastic problems in flight due to the aerodynamic forces. Aeroelasticity is the term concerned with the interacting phenomena between the elastic motions of structures and the resulting aerodynamic forces. In aeroelastic phenomena, there are many categories according to the physical features; flutter, divergence, gust responses, buffeting, limit cycle oscillations (LCO), etc. Even though all of these should be considered for aircraft design, flutter is the most dangerous problem because it can result in total structural failure in just a few seconds. Modern aircrafts are usually designed to cover a wide flight envelope, and they experience severe change in flow characteristics while they are passing through the transonic flow region. The flutter instability is usually aggravated in the transonic and low supersonic regions and it is closely related with the unstable movement of shock waves. Moreover, the fatigue induced by LCO of the air vehicles can reduce the operating range. LCO may occur due to the structural nonlinearity or the interaction between structures and nonlinear aerodynamic forces due to shock oscillation and flow separation in the transonic region. Thus, accurate prediction of aeroelastic characteristics such as flutter and LCO, is very important in the design state of aircraft, and

the analysis using linear theories has limits for the accurate prediction of the aeroelastic phenomena.

To perform the aeroelastic analysis in a transonic flow, CFD technique must be used to consider the moving shock. In particular, to analyze the nonlinearity in the flow field such as viscous effects, the Navier-Stokes equation with the turbulent model should be used to the aeroelastic analysis. However, it is difficult to use this theory for 3-dimensional wings with a control surface [1]. The arbitrary elastic motion with flap rotation gives the mesh and guaranteeing numerical instability problems. Moreover, when an aeroelastic analysis for the local motion of the control surface is conducted in the transonic flow region, heavy computation time is generally required to determine the aeroelastic boundary. Owing to the aforementioned problems, an aeroelastic analysis using the TSD code can have a strong computational advantage in various parametric studies. The TSD equation is widely recognized as one of the most efficient theories among the conventional CFD-based approaches. In addition, the TSD code does not require an additional grid re-meshing process since it uses the changes of the wing airfoil slopes at each wall grid point to simulate arbitrary wing surface motions [2].

In the structural point of view, structural nonlinearity is classified into distributed and concentrated one. The distributed nonlinearity is spread out over the entire structure such as the material and geometrical nonlinearities while the concentrated nonlinearity is placed in the specific location. The freeplay, friction and hysteresis are included in concentrated nonlinearity. Especially, freeplay is inevitable in control surfaces because of normal wear of components and manufacturing mismatches. Nonlinear aeroelastic analyses of a wing with concentrated nonlinearities have been investigated by several researchers [3-7]. Aeroelastic analyses for a geometrical structural nonlinearity have been studied by using the rotor blade of helicopter since 1970s. Generally, a blade is modeled by a beam to consider a large deformation. Aeroelastic analyses for a fixed-wing model have been performed for the high-altitude, long-endurance (HALE) aircraft with long-span wing [8-11].

In the present study, the aeroelastic characteristics are investigated for several wing models with control surface freeplay and high-aspect-ratio, and the aeroelastic analysis considering the transonic aerodynamic nonlinearity is performed for the full aircraft model which has the body, main wings, horizontal tails, vertical fin, launchers and several control surfaces.

<sup>1</sup> President of the Korean Society for Aeronautical and Space Sciences, and Professor at Dept. of Aerospace Eng., KAIST

<sup>2</sup> Research Assistant

## 2. THEORITICAL BACKGROUND

### 2.1. Nonlinear Aerodynamic Equation

Although the Navier-Stokes equations are the most accurate, many flow features depend on a precise evaluation of the viscous and turbulent terms. If the thickness of a wing section is small and there is no boundary layer separation, the viscosity has a small effect on the flow fields. If the viscous terms are removed from Navier-Stokes equations, the equation becomes an Euler equation. Furthermore, if the flow around the aircraft wing is irrotational and the perturbation is small, the TSD (Transonic Small Disturbance) theory can be applied. The TSD equation written in a conservative form is given by

$$(1) \frac{\partial f_0}{\partial t} + \frac{\partial f_1}{\partial x} + \frac{\partial f_2}{\partial y} + \frac{\partial f_3}{\partial z} = 0$$

where,

$$f_0 = -A\phi_t - B\phi_x, \quad f_1 = E\phi_x + F\phi_x^2 + G\phi_y^2, \\ f_2 = \phi_y(1 + H\phi_x), \quad f_3 = \phi_z$$

The above equations are given in a physical coordinate system,  $(x, y, z, t)$ .  $\Phi$  is the disturbance velocity potential. The coefficients  $A$ ,  $B$ , and  $E$  are defined as

$$(2) \quad A = M^2, \quad B = 2M^2, \quad E = 1 - M^2$$

Several choices are available for the definitions of  $F$ ,  $G$  and  $H$  depending on how the TSD equation is derived. The coefficients are given as

$$(3) \quad F = -\frac{1}{2}(\gamma + 1)M^2, \quad G = \frac{1}{2}(\gamma - 3)M^2, \\ H = -(\gamma - 1)M^2$$

where  $M$  is the free stream Mach number and  $\gamma$  is the ratio of specific heats.

The TSD equation is solved using a time-accurate AF (Approximate Factorization) method. The AF algorithm consists of a Newton linearization procedure coupled with an internal iteration technique. The solution process involves two steps. Firstly, a time linearization step is performed to determine an estimate of the potential field. Secondly, internal iterations are performed to minimize linearization and factorization errors [12].

### 2.2. Aeroelastic Equation of Motion

The aeroelastic equation of motion can be formulated by Hamilton principle for elastic models and is written in matrix form as follows:

$$(4) \quad [M_g]\{\ddot{q}(t)\} + [C_g]\{\dot{q}(t)\} + [K_g]\{q(t)\} = \{F_g(t)\}$$

where  $\{q(t)\}^T = [q(t)_1, q(t)_2, \dots, q(t)_n]$  is the generalized displacement vector and  $[M_g]$ ,  $[C_g]$ , and  $[K_g]$  express the generalized mass, damping, and stiffness matrices respectively.  $\{F_g(t)\}$  represents the generalized aerodynamic forces as follows:

$$(5) \quad F_{g_i}(t) = \frac{1}{2}\rho U^2 c_r^2 \int_{S^*} h_i(x^*, y^*) \Delta C_p(x^*, y^*, t) dS^*$$

where subscript ' $i$ ' indicates the influence mode and  $S^*$  is the non-dimensional plane area of wing.  $1/2\rho U^2 c_r^2$  is multiplied to make the dimensional force term because the inside of the integral is non-dimensional. In equations (4) and (5), symbol ' $t$ ' represents physical time, hence one must pay attention to the transition from non-dimensional time in the unsteady aerodynamics into physical time in the structural dynamics. The solution of equation (5) is obtained from the  $2 \times 2$  Gauss numerical integration method. The structural damping ratio is generally assumed to be 0.005 - 0.02.

Ordinary differential equations such as equation (4) can be reduced to the state vector forms for efficient numerical calculations and can be written as

$$(6) \quad \{\dot{x}(t)\} = [A]\{x(t)\} + [B]\{y(t)\}$$

where,

$$[A] = \begin{bmatrix} [0] & [I] \\ -[M_g]^{-1}[K_g] & -[M_g]^{-1}[C_g] \end{bmatrix}, \\ [B] = \begin{bmatrix} [0] \\ [M_g]^{-1} \end{bmatrix}$$

$$\{x(t)\} = \begin{Bmatrix} \{q(t)\} \\ \{\dot{q}(t)\} \end{Bmatrix}, \quad \{y(t)\} = \begin{Bmatrix} \{0\} \\ \{K_g(t)\} \end{Bmatrix}$$

A fifth-order Runge-Kutta method is used to solve the equation of motion.

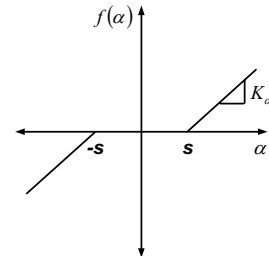


FIG 1. The resorting force due to structural nonlinearity.

The equation of motion of an aeroelastic system with structural nonlinearities can be written as

$$(7) \quad [M]\{\ddot{u}\} + [C]\{\dot{u}\} + \{R(u)\} = \{F(t, u, \dot{u})\}$$

where  $[M]$ ,  $[C]$ ,  $\{u\}$ , and  $\{F\}$  are mass matrix, damping matrix, displacement and external aerodynamic force vector, respectively.  $\{R(u)\}$  is the restoring force vector including structural nonlinearities.  $\{R(u)\}$  is expressed as

$$(8) \quad \{R(u)\} = [K]\{u\} + \{f(\alpha)\}$$

where  $[K]$  is the linear stiffness matrix,  $\{f(\alpha)\}$  is the restoring force vector due to structural nonlinear factors and is given as

$$(9) \quad f(\alpha) = \begin{cases} K_\alpha(\alpha - s) & : \alpha > s \\ 0 & : -s \leq \alpha \leq s \\ K_\alpha(\alpha + s) & : \alpha < -s \end{cases}$$

where  $K_\alpha$ ,  $\alpha$ , and  $s$  are linear stiffness, flap angle and freeplay angle in FIG.1, respectively.

Usually, the aeroelastic analysis is conducted by using a modal approach with limited number of low frequency modes to reduce the computational time. In general, the normal mode approach cannot be used directly due to stiffness variation for air vehicle wings with freeplay. To overcome this difficulty, the fictitious mass (FM) method is applied [13]. It is discussed the application procedure of the FM method to a wing with freeplay in Ref.7. After the modal matrix,  $[\Phi_b]$ , is obtained from the fictitious mass model, the displacement vector can be expressed as

$$(10) \{u(t)\} = [\Phi_b] \{q(t)\}$$

where  $\{q\}$  is the generalized displacement vector. Transformation of equation (7) into the modal coordinate system gives the following equation

$$(11) [M_g] \{\ddot{q}(t)\} + [C_g] \{\dot{q}(t)\} + \{R_g(u)\} = \{F_g(t)\}$$

where  $\{R_g\}$  is the generalized restoring vector defined as  $[\Phi_b]^T [K] [\Phi_b] \{q\} - [\Phi_b] \{f(\alpha)\}$ . The theoretical background and verification are discussed in Ref.7.

To analyze a high-aspect-ratio wing structure using the large deflection beam theory, following assumptions are introduced: there is no deformation on the cross sectional plane. Hence, one-dimensional model is available along the beam axis. The beam can have initial curvature and twist. Initial curvature, however, is small like a practical wing. The strain level remains small even if a large deflection occurs. Then, the wing can be modeled as a cantilever beam.

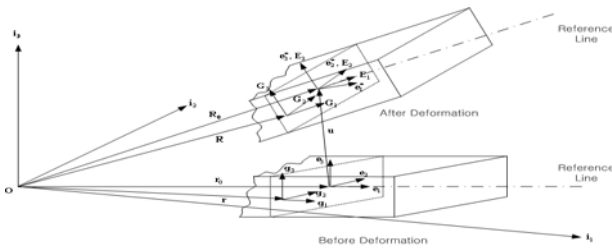


FIG 2. Geometry and coordinate systems before and after deformation.

Consider the naturally curved and twisted beam as depicted in FIG.2. Assuming that initial curvatures are small and shearing strains are much smaller than unity in the Green-Lagrangian strain components, strain-displacement relations are represented as those in Ref.14. The geometrical nonlinearities are described by coordinate transformation matrices using the Euler angles in the present large deflection beam theory.

$$(12) \begin{aligned} e_i^* &= t_e(x_1) e_i = T(x_1) i_i \\ T(x_1) &= t_e(x_1) t_g(x_1) \end{aligned}$$

where the triad  $i_i$  is fixed in a reference frame that rotates at a constant angular velocity with respect to the inertia frame; the triad  $e_i$  is attached to a reference line along the axis of the undeformed beam; and the triad  $e_i^*$  is attached to a reference line along the axis of the deformed beam. The transformation matrices  $t_e$ ,  $t_g$ , and  $T$  are functions of the curvilinear axial coordinate  $x_1$ .

To calculate the strain in the curvilinear coordinate, Green-Lagrange strain tensor is introduced. By the assumption of

small initial curvature of the beam, high order terms in Green-Lagrange strain can be neglected. Thus, engineering strains are obtained as follows:

$$(13) \begin{aligned} \varepsilon_{11} &= \hat{e}_{11} + x_3 \kappa_2 - x_2 \kappa_3 + \omega_1', & \varepsilon_{22} &= \omega_{2,2}, & \varepsilon_{33} &= \omega_{3,3} \\ \gamma_{12} &= 2\hat{e}_{12} - x_3 \kappa_1 + \omega_{1,2} + \omega_2', & \gamma_{23} &= \omega_{2,3} + \omega_{3,2}, \\ \gamma_{13} &= 2\hat{e}_{13} - x_2 \kappa_1 + \omega_{1,3} + \omega_3', \\ \kappa_i &= K_i - k_i \end{aligned}$$

where  $x_1$ ,  $x_2$ , and  $x_3$  are curvilinear coordinates.  $w_1$ ,  $w_2$ , and  $w_3$  are the general warping displacements of an arbitrary point on the cross section. The force strains,  $(\hat{e}_{11}, 2\hat{e}_{12}, 2\hat{e}_{13})$  and moment strains,  $(\kappa_1, \kappa_2, \kappa_3)$  components are given in Ref.15. Herein,  $( )'$  means the derivative with respect to  $x_1$  and  $( )_i$  means the derivatives with respect to  $x_i$ ,  $i = 2, 3$ . Through a quasi-linear approximation, the three-dimensional kinematics is divided two-dimensional cross-sectional analysis and the one-dimensional global analysis.

The equation of motion can be obtained using the Hamilton's principle as follows:

$$(14) \int_{t_2}^{t_1} \sum_{i=1}^m (\delta U_i - \delta T_i - \delta W_i) dt = 0$$

where  $\delta U_i$ ,  $\delta T_i$ , and  $\delta W_i$  are the variation of stain energy, the variation of kinetic energy, and the virtual work done by external forces. The nonlinear finite element equation of motion can be obtained in the matrix form,

$$(15) [M(q)] \{\ddot{q}\} + P(q) - P_A(q) = \{0\}$$

where  $M(q)$  and  $P(q)$  are the mass and the internal elastic force vector.  $P_A(q)$  is external forces by aerodynamic forces. Newton-Raphson method combined with the line search method to improve convergence and reliability is applied.

### 3. VERIFICATION OF AEROELASTIC ANALYSIS SYSTEM

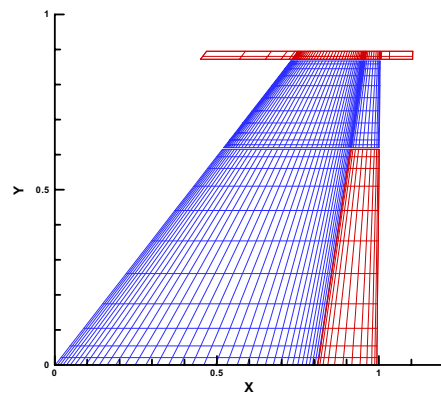


FIG 3. Aerodynamic grid for the F-16 main wing model.

The present aeroelastic analysis system using the TSD equation is verified with the flight test data of the F-16 wing model, which are obtained from Ref.16. The appendix in the reference presents three mode shape data (wing bending, torsion and forward wing torsion modes). Figure 3 shows the TSD grid for the aerodynamic analysis. Each

aerodynamic grid of  $x$  and  $y$  direction is clustered on the near leading and trailing edge as well as the hinge part. The wing model has a shape of a NACA 64A204 airfoil. To derive the mode spline, the wing part should be divided into three parts; the wing, the control surface and the launcher. After obtaining the mode spline, the divided parts are re-united in the aerodynamic coordinate. Figure 4 shows the splined mode shapes into the aerodynamic grid. From the first mode to the third mode, each mode shape is wing bending, torsion, and forward wing torsion, respectively.

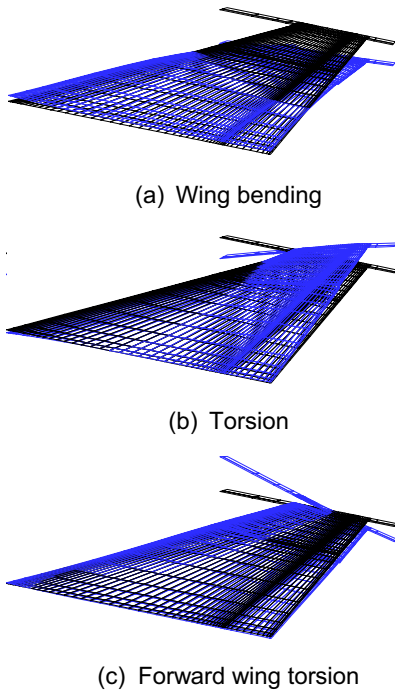


FIG 4. Aerodynamic grid for the F-16 main wing model.

Flutter analysis	Mode	Wing bending	Torsion	Forward wing torsion
		Freq. (Hz)	9.191	9.964
DLM [16]	$V_f$ (KCAS)	745.2	.	442.4
	$F_f$ (Hz)	9.37	.	10.17
Flight test [16]	$V_f$ (KCAS)	585	.	.
	$F_f$ (Hz)	9.5	.	.
Present	$V_f$ (KCAS)	628.2	.	.
	$F_f$ (Hz)	9.29	.	.

TAB 1. Comparisons of flutter velocity and frequency between experiment and analyses.

The present aeroelastic analysis code using the TSD equation gives the accurate flutter velocity and frequency and the results are compared with the DLM results and the flight test data. The analysis and experimental results for the flutter velocity and frequency are arranged in TAB.1.

The flutter speeds are expressed by the knots calibrated airspeed. The present aeroelastic result using the TSD equation shows the closer flutter speed to flight test than the DLM analysis result on the wing-bending mode [17].

## 4. RESULTS AND DISCUSSION

### 4.1. Aeroelastic Analysis of Wing Model with Control Surface Freeplay

The numerical nonlinear aeroelastic characteristics are investigated for the wing with control surface freeplay. The wing has a root chord length of 0.6396 m, a span length of 0.6226 m. The hinge axis is located at 82 % chord section and 0.3571 m long as shown in FIG.5. For the wing section, 4 % biconvex airfoil is used.

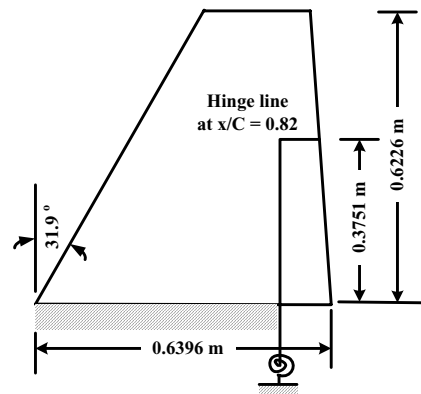
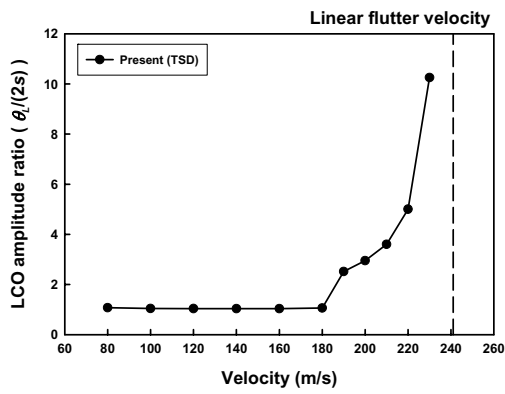
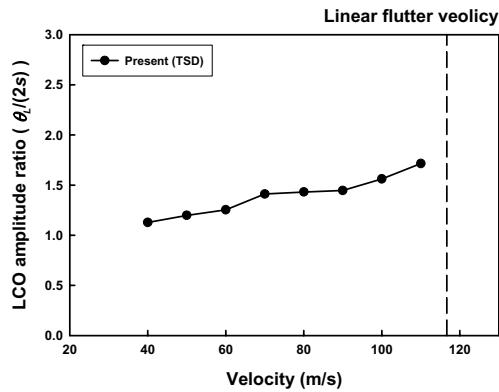


FIG 5. Geometrical configuration of the wing with control surface.

Figure 6 shows the Limit Cycle Oscillations (LCO) amplitude ratio at the flow velocity of  $M = 0.70$  and  $0.95$ . Linear flutter speed means the flutter boundary of the linear structural model with zero freeplay angle. The freeplay angle,  $s$  of  $0.125^\circ$  and angle of attack of  $0^\circ$  are used for all cases. The initial disturbance is given by flap angle,  $\theta_0 = 0.25^\circ$ , defined as the angular displacement about the hinge axis with the rigid body rotation of the wing. The  $\theta_L$  is the flap angle at the hinge axis. From  $V = 80$  to  $180$  m/s, the LCO amplitude ratio is about one. It means that aeroelastic responses of flap angle are bounded to freeplay angle. As airflow velocity increases, the LCO amplitudes increase. At the airflow velocity of around  $230$  m/s, unstable response is initiated. At  $M = 0.95$ , the LCO amplitude is slightly increased. Around the linear flutter velocity, the LCO amplitude is diverged. Figure 7 shows the phase plot at the end of the wing and flap trailing edge. In present study, phase plot is illustrated after the transient response. The square and circle symbols stand for the maximum flap and wing displacement, respectively. The phase differences can be referred to phase plot. Figure 7 demonstrate the phase plot at  $M = 0.7$ . At  $V = 160$  m/s the displacement of the wing is larger than that of flap. Also, the vibrations of the wing and flap are in the same phase motion. At  $V = 200$  m/s, on the other hand, the entirely different phenomena happen comparing to  $V = 160$  m/s. Such a dynamic response is similar to the onset of flutter.

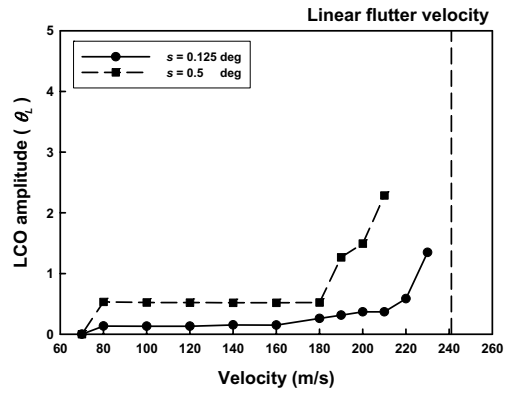


(a)  $M = 0.70$

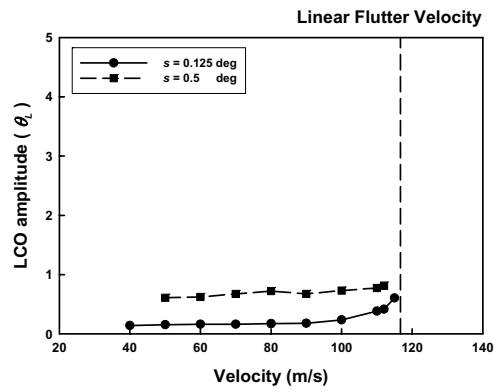


(b)  $M = 0.95$

FIG 6. Velocity vs. the LCO amplitude ratio.

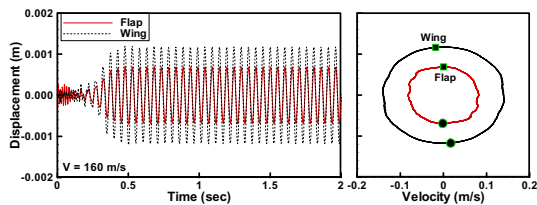


(a)  $M = 0.70$

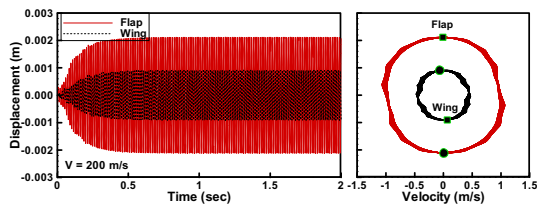


(b)  $M = 0.95$

FIG 8. Comparisons of the LCO amplitude with freeplay angle changes.



(a)  $V = 160$  m/s



(b)  $V = 200$  m/s

FIG 7. Aeroelastic response and phase plots at wing and flap tips at  $M = 0.7$ .

Figure 8 shows comparisons of the LCO amplitudes for  $s = 0.125^\circ$  and  $0.5^\circ$ . Initial flap angle is  $1.0^\circ$  at all cases in the subsonic flow region, and the initiation velocities of the LCO are not changed. At the freeplay angle of  $0.5^\circ$ , the LCO amplitude is always larger than that of  $0.125^\circ$ . The flutter boundary of  $s = 0.5^\circ$  is reduced about 10 % comparing with that of  $s = 0.125^\circ$ . At  $M = 0.95$  and  $s = 0.5^\circ$  chaotic responses are observed at low velocity. For a higher freeplay angle, the LCO amplitude is higher.

## 4.2. Aeroelastic Analysis of High-Aspect-Ratio Wing Model

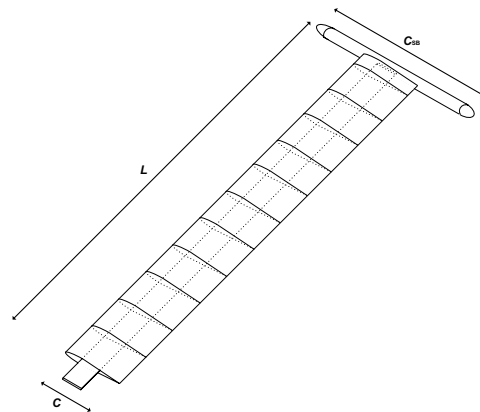
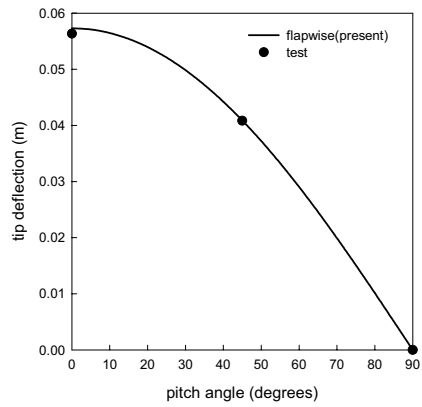
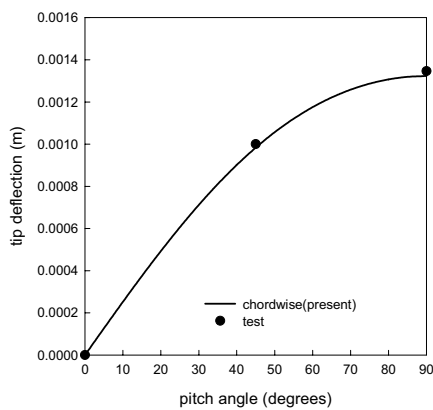


FIG 9. The high-aspect-ratio wing model.

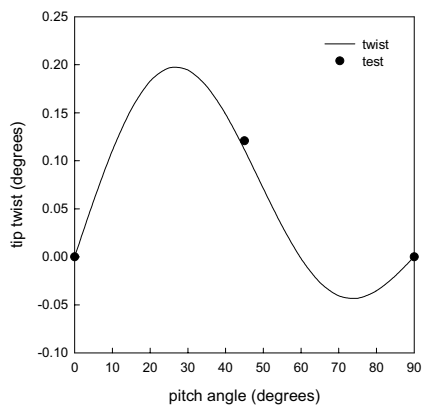
The nonlinear static aeroelastic analysis for a high-aspect-ratio wing is performed. The TSD theory for the aerodynamic analysis and the large deflection beam theory considering a geometrical nonlinearity for the structural analysis are applied for the aeroelastic analysis. The high-aspect-ratio wing model has a root chord length( $C$ ) of 0.0508 m, a span length( $L$ ) of 0.4508 m and a aspect-ratio of about 9. Figure 9 shows the configuration of the analysis model. More detailed information of the wing configuration is discussed in Ref.10.



(a) Flap-wise deflection



(b) Chord-wise deflection

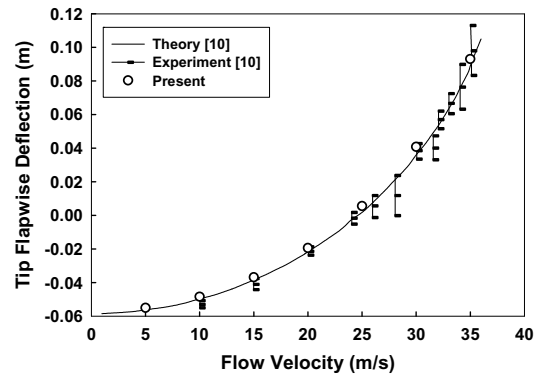


(c) Twist angle

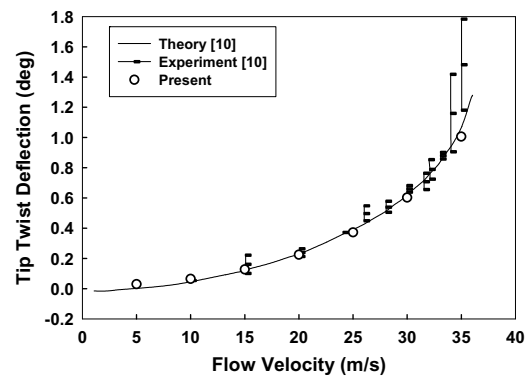
FIG 10. Static displacement of the wing tip under gravity loading.

Figure 10 shows the comparisons of static deflections between present results and experimental data which are obtained from Ref.10. For investigating the static flap-wise and chord-wise bending deflections and twist at tip vs.  $\theta_0$  under gravity effect only, three pitch angles,  $\theta_0 = 0^\circ, 45^\circ, 90^\circ$ , are selected. Herein, flap-wise bending refers to bending perpendicular to the wing chord and chord-wise bending has the parallel direction with the wing plane. When pitch angle is equal to zero, the flap deflections are dominant. As pitch angle increases, flap deflection

decreases. From the comparisons between the present and experimental results, the nonlinearity effects of the large deflection are well described by the present analyses. The aerodynamic grids contain  $80 \times 78 \times 40$  node points in  $x, y,$  and  $z$  directions, respectively. Although the experimental model has a tip store, its aerodynamic effect is negligible. Thus, the tip store is ignored in the aerodynamic analysis. When the angle of attack is  $2.2^\circ$ , the flap deflection and twist angle at the tip are shown in FIG.11. In the higher velocity range, the experimental data fluctuation augments due to greater aerodynamic interference. Both the tip deflection and twist angle increase by the aerodynamic forces as the change of flow velocity.



(a) Flap-wise displacement



(b) Twist angle

FIG 11. Static aeroelastic analysis results at  $\theta_0 = 2.2^\circ$ .

### 4.3. Aeroelastic Analysis of Full Aircraft Model

One of the advantages of the TSD equation in the aeroelastic analysis is that it alone can be applied to a realistic aircraft model considering all wings and control surfaces. The application using the Euler and Navier-Stokes aeroelastic programs would be impractical because of the impracticable computing time and mesh treatments on joint parts between control surface and the remaining parts. The TSD code is widely recognized as one of the most efficient and robust tools among conventional CFD-based computational aeroelasticity.

The present aeroelastic program using TSD theory is applied to the T-50 supersonic aircraft model. The T-50 is a supersonic advanced jet trainer developed by KAI

(Korea Aerospace Industries, Ltd.). The aircraft model includes the body, main wings, horizontal tails, vertical fin, launchers and several control surfaces.

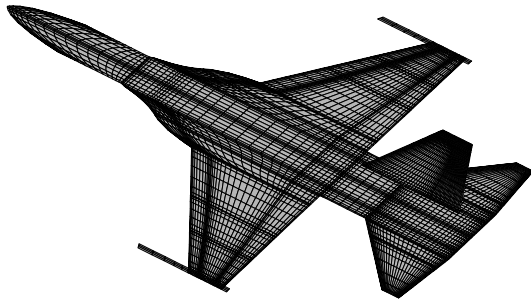


FIG 12. Aerodynamic grid of the full aircraft model.

Figure 12 shows the aeroelastic grid system of the full aircraft model. The airfoils of the main wings are NACA 64 series. Each of the horizontal and vertical tails has a biconvex airfoil.

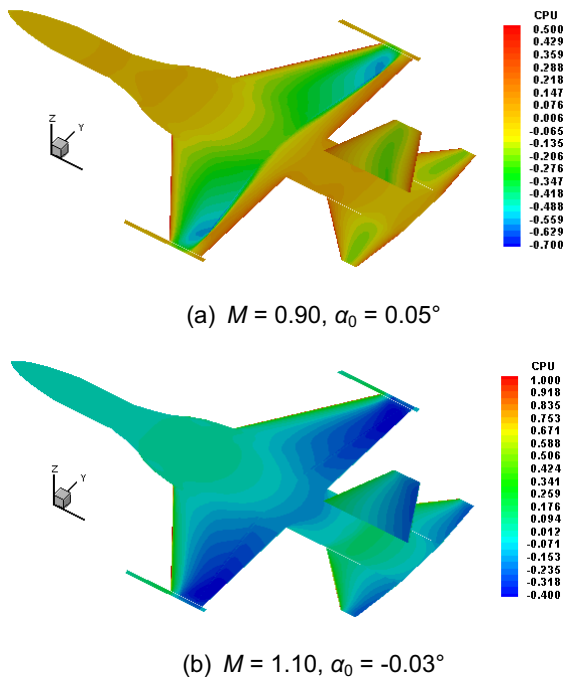


FIG 13. Steady pressure contours at  $M = 0.90$  and  $1.10$ .

Steady aerodynamic pressure was computed by the TSD equation. Figure 13 shows the steady pressure contours at  $M = 0.90$  and  $1.10$ . Each angle of attack is  $0.05^\circ$  and  $-0.03^\circ$ , respectively. At  $M = 0.90$ , the normal shock waves are on the main wings, horizontal and vertical tails. Steady pressure comparisons between the analytic results and experimental data are presented in FIG.14 for five span stations of the main wing at  $M = 0.80$  and  $\alpha_0 = 0^\circ$ . The present results generally agree well with the experimental data [18]. Figure 15 shows steady pressure comparisons for the three stations of the vertical fin. The analytic results generally agree well with the experimental data. At  $M = 0.95$  and  $\alpha_0 = 0^\circ$ , there is a moderately strong shock wave on the vertical fin surface.

Aeroelastic solutions are obtained by solving the aeroelastic equation of motion and can be represented by the superposition of mode shapes. The mode shapes and natural frequencies of the aircraft model have been

obtained via free vibration analysis, using MSC /NASTRAN<sup>TM</sup>, and 28 elastic modes are applied to the aeroelastic analysis.

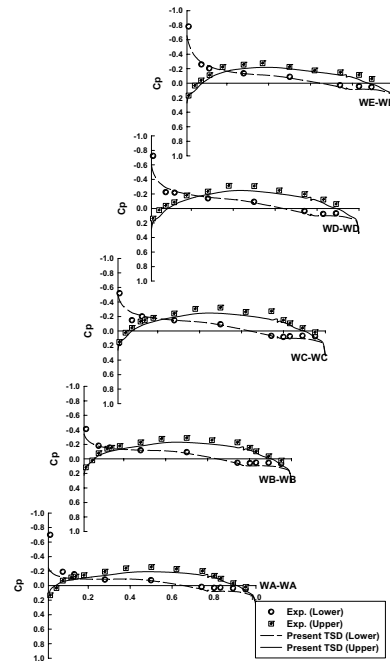


FIG 14. Comparisons of steady pressure coefficient on the main wing surface at  $M = 0.80$  and  $\alpha_0 = 0.0^\circ$ .

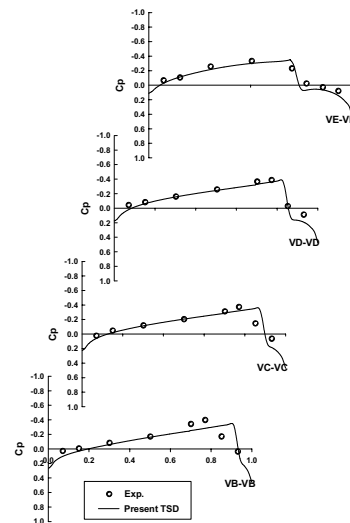


FIG 15. Comparisons of steady pressure coefficient on the vertical tail surface at  $M = 0.95$  and  $\alpha_0 = 0.0^\circ$ .

Generally, multi-disciplinary problems, including aeroelastic analysis, require a data transfer stage between mismatched grid systems such as the structural grid and the aerodynamic grid because those points have been subjected to different engineering considerations. For example, the aerodynamic load is usually subjected to the external surface, whereas the load-carrying components are placed inside the wing or fuselage. This gives rise to the necessity of data transfer between the two different systems. In the present aeroelastic analysis, the displacements of the structural grid are interpolated to the aerodynamic grid by the Infinite Plate Spline (IPS) method. Figure 16 shows the interpolated mode shapes of several

symmetric and anti-symmetric modes. If there is a discontinuity, such as flap, then the wing structure is divided into parts: the control surface and the remaining part of the wing. Therefore, each part must be transferred independently and then superposed.

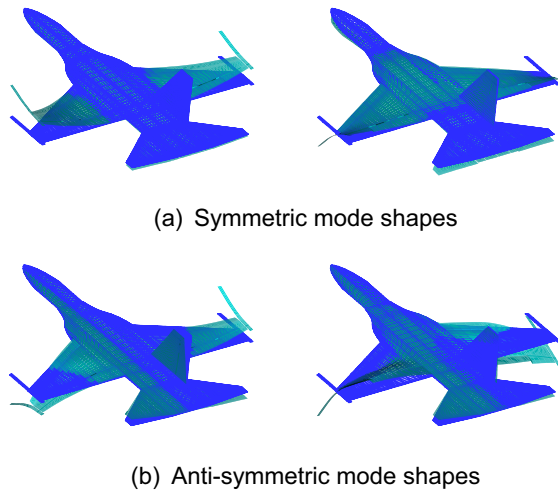


FIG 16. Structural mode shapes of the full aircraft model.

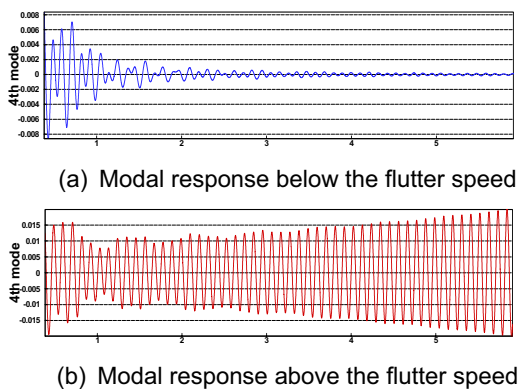


FIG 17. Aeroelastic time responses at  $M = 0.90$ .

In the time-domain approach, the aeroelastic instabilities can be predicted by simulating whether the response is decaying or diverging. Figure 17 shows aeroelastic responses above and below the flutter speed in the modal coordinate. A flutter boundary exists between the two dynamic pressures corresponding to these responses. It is sometimes difficult to obtain a neutral response which indicates flutter boundary. Hence, the aeroelastic analysis should be repeated several times or else an additional signal processing technique will be required to estimate the flutter point. In this study, damping ratio and frequency are calculated using the Moving Block Method (MBM), and the flutter boundaries are predicted by an interpolation of damping ratios.

## 5. CONCLUSIONS

In this study, the aeroelastic analyses for several models considering aerodynamic nonlinearity as well as concentrated and distributed structural nonlinearities are

performed. In the aerodynamic analysis, the transonic small disturbance (TSD) equation is used for efficient computing time and easy treatment of control surfaces. For the aeroelastic analysis of wing model with concentrated structural nonlinearity such as control surface freeplay, the limit cycle oscillations (LCO) characteristics are investigated by comparing the LCO amplitude ratio and displacement of flap and wing as the change of air flow velocity and freeplay angle. To consider the control surface freeplay, the restoring force vector and the fictitious mass method are applied to the aeroelastic analysis system. Also, the aeroelastic analysis for distributed structural nonlinearity is performed. The geometrical nonlinear structural results are obtained from the large deflection beam theory for the high-aspect-ratio wing model. For the high-aspect-ratio wing model, the present structural analysis system and the aeroelastic analysis system are validated. Also, the TSD code is used for the nonlinear aeroelastic analysis of the full aircraft model in the transonic region. The model includes the body, main wings, horizontal tails, vertical fin, launchers and several control surfaces. The aeroelastic analysis results were quite accurate and the developed flutter analysis system based on the TSD theory is well suited for practical applications of the complex aircraft models.

## ACKNOWLEDGEMENTS

This work was supported by Korea Aerospace Industries, Ltd., Defense Acquisition Program Administration and Agency for Defense Development under the contract UD070041AD.

## REFERENCES

- [1] D.H. Kim, Y.M. Park, I. Lee, and O.J. Kwon, "Nonlinear Aeroelastic Computation of a Wing/Pylon/Finned-Store Using Parallel Unstructured Euler Solver," *AIAA Journal*, Vol. 43, No. 1, pp. 53-62, 2005.
- [2] H.J. Kwon, D.H. Kim, and I. Lee, "Frequency and Time Domain Flutter Computations of a Wing with Oscillating Control Surface Including Shock Interference Effects," *Aerospace Science and Technology*, Vol. 8, pp. 519-532, 2004.
- [3] R.M. Laurenson and R.M. Trn, "Flutter Analysis of Missile Control Surfaces Containing Structural Nonlinearities," *AIAA Journal*, Vol. 18, No. 10, pp. 1245-1251, 1980.
- [4] S.H. Kim and I. Lee, "Aeroelastic Analysis of a Flexible Airfoil with a Freeplay Non-linearity," *Journal of Sound and Vibration*, Vol. 193, No. 4, pp. 823-846, 1996.
- [5] K.A. Kousen and O.O. Bendiksen, "Limit Cycle Phenomena in Computational Transonic Aeroelasticity," *Journal of Aircraft*, Vol. 31, No. 6, pp. 1257-1263, 1994.
- [6] J.S. Bae, D.J. Inman, and I. Lee, "Effects of Structural Nonlinearity on Subsonic Aeroelastic Characteristics of an Aircraft Wing with Control Surface," *Journal of Fluids and Structures*, Vol. 19, No. 6, pp. 747-763, 2004.

- [7] J.H. Yoo, Y.K. Park, I. Lee, and J.H. Han, "Aeroelastic Analysis of a Wing with Freeplay in the Subsonic/Transonic Regions," *JSME International Journal, Series B: Fluids and Thermal Engineering*, Vol. 48, No. 2, pp. 208-211, 2005.
- [8] C. Pendaries, "From the HALE Gnopter to the Ornithopter How to Take Advantage of Aircraft Flexibility," *AIAA Paper A98-31751*, 1998.
- [9] M.J. Patil, D.H. Hodges, and C.E.S. Cesnik, "Nonlinear Aeroelasticity and Flight Dynamics of High-Altitude Long-Endurance Aircraft," *Journal of Aircraft*, Vol. 38, No. 1, pp. 88-94, 2001.
- [10] D.M. Tang and E.H. Dowell, "Experimental and Theoretical Study on Aeroelastic Response of High-Aspect-Ratio Wings," *AIAA Journal*, Vol. 39, No. 8, pp. 1430-1441, 2001.
- [11] J.H. Yoo, I.G. Lim, and I. Lee, "Nonlinear Static Aeroelastic Analysis of a High-Aspect-Ratio Wing with Large Deflection Theory," *Journal of Korean Society for Aeronautical and Space Science*, Vol. 34, No. 3, pp. 31-36, 2006.
- [12] J.T. Batina, "Unsteady Transonic Algorithm Improvement for Realistic Aircraft Applications," *Journal of Aircraft*, Vol. 26, No. 2, pp. 131-139, 1989.
- [13] M. Karpel and C.D. Wieseman, "Modal Coordinates for Aeroelastic Analysis with Large Local Structural Variation," *Journal of Aircraft*, Vol. 31, No. 2, pp. 396-400, 1994.
- [14] O.A. Bauchau and C.H. Hong, "Nonlinear Composite Beam Theory," *Journal of Applied Mechanics*, Vol. 55, pp. 156-163, 1988.
- [15] S.M. Jeon, M.H. Cho, and I. Lee, "Static and Dynamic Analysis of Composite Box Beams using Large Deflection Theory," *Computers and Structures*, Vol. 57, No. 4, pp. 635-642, 1995.
- [16] C.M. Denegri, Jr., "Limit Cycle Oscillation Flight Test Results of a Fighter with External Stores," *AIAA paper, AIAA-2000-1394*, 2000.
- [17] I. Lee, H.J. Kwon, J.Y. Kim, J.H. Yoo, S.K. Paek, Y.I. Kim, and J.S. Bae, "Transonic Flutter Prediction of Supersonic Jet Trainer with Various External Store Configurations," *47th AIAA/ASME/ASCE/AHS/ASC Structures, Structural Dynamics & Materials Conference*, Newport, Rhode Island, May 2006.
- [18] J.H. Yoo, D.H. Kim, H.J. Kwon, and I. Lee, "Nonlinear Aeroelastic Simulation of a Full-Span Aircraft with Oscillating Control Surfaces," *Journal of Aerospace Engineering*, Vol. 18, No. 3, pp.156-167, 2005.